AMERICAN SOCIETY FOR MICROBIOLOGY | Molecular and Cellular Biology®

RESEARCH ARTICLE

Targeted Degradation of Glucose Transporters Protects against Arsenic Toxicity

Marco Jochem,[a] Lukas Ende,[a] Marta Isasa,[b]* Jessie Ang,[a] Helena Schnell,[a] Angel Guerra-Moreno,[a] Yagmur Micoogullari,[a] Meera Bhanu,[a] Steven P. Gygi,[b] John Hanna[a]

[a]Department of Pathology, Brigham and Women's Hospital and Harvard Medical School, Boston, Massachusetts, USA
[b]Department of Cell Biology, Harvard Medical School, Boston, Massachusetts, USA

ABSTRACT The abundance of cell surface glucose transporters must be precisely regulated to ensure optimal growth under constantly changing environmental conditions. We recently conducted a proteomic analysis of the cellular response to trivalent arsenic, a ubiquitous environmental toxin and carcinogen. A surprising finding was that a subset of glucose transporters was among the most downregulated proteins in the cell upon arsenic exposure. Here we show that this downregulation reflects targeted arsenic-dependent degradation of glucose transporters. Degradation occurs in the vacuole and requires the E2 ubiquitin ligase Ubc4, the E3 ubiquitin ligase Rsp5, and K63-linked ubiquitin chains. We used quantitative proteomic approaches to determine the ubiquitinated proteome after arsenic exposure, which helped us to identify the ubiquitination sites within these glucose transporters. A mutant lacking all seven major glucose transporters was highly resistant to arsenic, and expression of a degradation-resistant transporter restored arsenic sensitivity to this strain, suggesting that this pathway represents a protective cellular response. Previous work suggests that glucose transporters are major mediators of arsenic import, providing a potential rationale for this pathway. These results may have implications for the epidemiologic association between arsenic exposure and diabetes.

KEYWORDS Rsp5, arsenic, glucose transporter, protein degradation, ubiquitin

The trivalent metalloid arsenic (arsenite) is a ubiquitous environmental toxin with broad public health relevance. Exposure has been associated with various cancer types, including those of skin, lung, bladder, and kidney (1), as well as an increased risk of diabetes (2–4). Exposure is mainly through contaminated groundwater, which occurs naturally or as a consequence of human activity. In the past, arsenic was widely used as a pesticide, an herbicide, and a wood preservative, among many other applications (5). Thus, arsenic continues to contaminate water supplies, even though its commercial use in the United States has been greatly curtailed. Indeed, arsenic currently ranks first on the Superfund Substance Priority List (6).

Arsenic toxicity is likely pleiotropic in nature (7). DNA damage and oxidative damage through the production of reactive oxygen species are thought to be major contributors. An emerging aspect of arsenic's toxicity relates to its ability to induce protein misfolding, sometimes referred to as proteotoxicity (8, 9). This may be related to arsenic's ability to covalently interact with free thiol groups in amino acid side chains, altering protein structure (10, 11). Remarkably, arsenite is also a highly effective FDA-approved therapy for acute promyelocytic leukemia, where, in combination with a second drug (all-*trans*-retinoic acid), it has helped transform this cancer from one that was typically fatal to one in which cure rates now exceed 90% (12). This cancer is driven by a cytogenetic translocation-derived fusion protein, PML-retinoic acid receptor α

Citation Jochem M, Ende L, Isasa M, Ang J, Schnell H, Guerra-Moreno A, Micoogullari Y, Bhanu M, Gygi SP, Hanna J. 2019. Targeted degradation of glucose transporters protects against arsenic toxicity. Mol Cell Biol 39:e00559-18. https://doi.org/10.1128/MCB.00559-18.

Address correspondence to John Hanna, jwhanna@bwh.harvard.edu.

* Present address: Marta Isasa, C4 Therapeutics, Watertown, Massachusetts, USA.

Received 26 November 2018
Returned for modification 12 December 2018
Accepted 12 March 2019
Accepted manuscript posted online 18 March 2019
Published 30 April 2019

(PML-RARα). Arsenic covalently binds to free cysteine groups in this fusion protein, which triggers destruction of the protein by the ubiquitin-proteasome system (13).

The essentially universal nature of arsenic toxicity is emphasized by the fact that organisms from bacteria to humans have evolved dedicated arsenic detoxification pathways. These include modulation of arsenic import, stimulation of arsenic efflux, chemical modification of arsenic (e.g., glutathionylation), and sequestration of arsenic (1, 5). Arsenic has no known metabolic or nutritional role. Thus, its uptake into cells appears adventitious (1). In budding yeast (*Saccharomyces cerevisiae*), two routes of arsenic import have been described. The first is through the glycerol transporter Fps1 (14). The second is through multiple members of the family of hexose transporters whose normal function is to promote the uptake of various six-carbon sugars—such as glucose, galactose, and maltose—which are major substrates for energy production (15). Of the 18 hexose transporters (Hxt1 to Hxt17, Gal2), Hxt1 to Hxt7 account for most of the glucose import, and a mutant lacking *hxt1* to *hxt7* (the *hxt1-7*Δ mutant) cannot grow on medium containing glucose as the sole carbon source (16). These transporters share common structural features, being integral membrane proteins with 12 transmembrane domains (17). They show various affinities for glucose, and cells have developed complex transcriptional and posttranscriptional regulatory pathways to control the abundance of individual transporters in response to glucose availability (17). Under glucose-replete conditions, glucose uptake is primarily mediated by low-affinity transporters. Conversely, under low-glucose conditions, higher-affinity transporters are induced to mediate import. Arsenic import appears to be an evolutionarily conserved property of glucose transporters, as the mammalian transporter Glut1 also imports arsenic (18, 19).

We recently determined the cellular response to trivalent arsenic using a proteomic approach (9). A surprising and dramatic finding was that a subset of glucose transporters was among the most downregulated proteins in the cell upon arsenic exposure. Here we sought to understand the molecular basis for this observation. We provide evidence that arsenic-induced downregulation of glucose transporters represents a protective cellular response and is mediated by a pathway of ubiquitin-dependent vacuolar protein degradation, which we have characterized in detail.

RESULTS

Arsenite-induced downregulation of glucose transporters. We recently reported a proteomic analysis of the cellular response to arsenite (9). Using tandem mass tag (TMT)-based mass spectrometry, we quantitated the relative change in protein abundance of 4,563 proteins (of approximately 6,000 in this organism) at 0, 1, and 4 h after arsenite treatment (1 mM) and with biological triplicates. We showed that cells that had been treated under these conditions for up to 4 h resumed growth with a normal doubling time within 1 to 2 h of arsenic washout, indicating that the proteomic changes observed represent a physiologic stress response rather than a reflection of nonspecific changes in dead or dying cells (9).

This analysis revealed a dramatic and comprehensive remodeling of the proteome, with approximately 1,000 proteins showing a significant change in protein abundance. Pathways of protein homeostasis (proteostasis), including the ubiquitin-proteasome pathway, autophagy, and the ribosome, were particularly affected (9). A surprising finding from this proteomic data set was that a subset of glucose transporters was among the most downregulated proteins in the cell (Fig. 1A). The most affected were the high-affinity transporters Hxt2, Hxt6, and Hxt7. Indeed, at 4 h after treatment, Hxt2 and Hxt6 represented the 2nd and 5th most downregulated proteins, respectively, of 4,563 detected. Hxt1, Hxt3, and Hxt4 also showed some downregulation, but this appeared to be less dramatic than that seen with Hxt2, Hxt6, and Hxt7. Hxt5 showed no reduction in protein levels.

We sought to verify the proteomic data by standard immunoblot analysis. We chose Hxt2 and Hxt7 for further study (Hxt6 and Hxt7 are nearly identical at the amino acid level). To allow for detection, we inserted a 3× hemagglutinin (HA) tag at the 3′ end

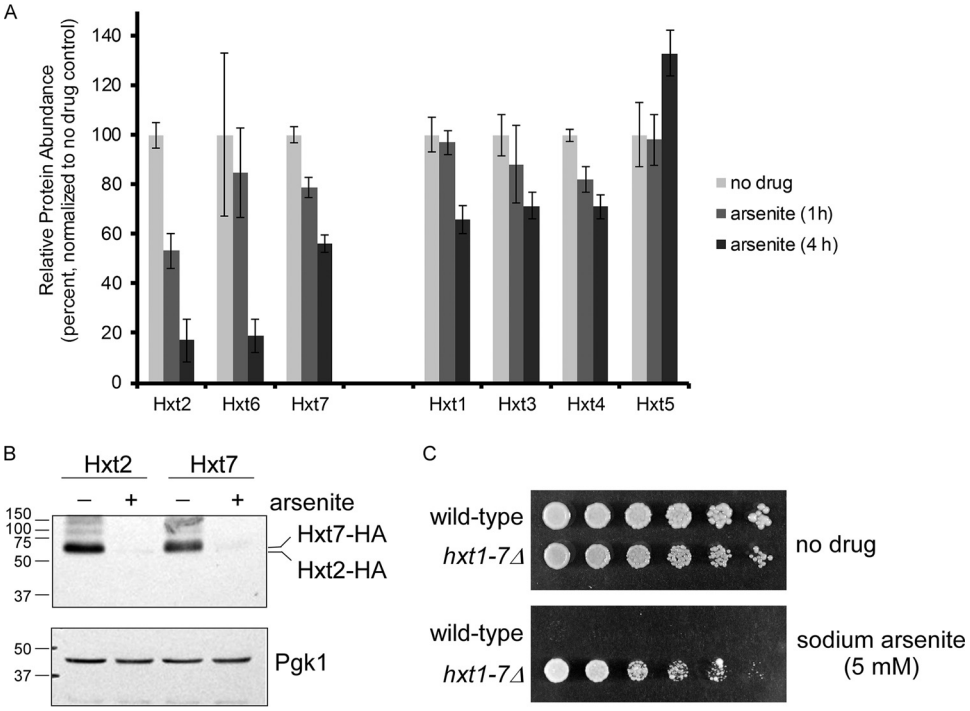

FIG 1 Arsenic-induced downregulation of glucose transporters. (A) Relative protein abundance of glucose transporters Hxt1 to Hxt7 determined by proteomic analysis at 0, 1, and 4 h after treatment with sodium arsenite (1 mM). Error bars represent standard deviations for triplicate cultures. Note that because of the high sequence similarity between Hxt6 and Hxt7 (only 1 amino acid difference), only one unique peptide could be assigned to Hxt6, while all other peptides were assigned to Hxt7. Thus, the result for Hxt7 likely reflects results for a combination of peptides from Hxt6 and Hxt7. (B) Downregulation of Hxt2-HA and Hxt7-HA in response to sodium arsenite, as determined by SDS-PAGE followed by immunoblot analysis. Proteins were extracted from log-phase yeast cells before (lanes −) and 3 h after (lanes +) treatment with 1 mM sodium arsenite. (Top) Anti-HA antibody; (bottom) Pgk1 (loading control). Numbers on the left are molecular masses (in kilodaltons). (C) Strong resistance of the *hxt1-7*Δ mutant to arsenite toxicity. Cells were spotted in a 3-fold serial dilution series on plates containing or lacking sodium arsenite (5 mM) and incubated at 30°C for 2 (no drug) or 5 (arsenite) days. Because the *hxt1-7*Δ mutant cannot grow with glucose as the sole carbon source, the medium contained both glucose and maltose (2% each).

of each gene. These proteins were thus expressed from their endogenous genomic loci and without alteration of their upstream promoter elements. We cultured cells and prepared whole-cell extracts before and after arsenite treatment. We analyzed the extracts by sodium dodecyl sulfate-polyacrylamide gel electrophoresis (SDS-PAGE), followed by immunoblotting with anti-HA antibodies. As shown in Fig. 1B, there was a dramatic reduction in Hxt2 and Hxt7 protein levels after arsenic treatment. This effect was specific, as an unrelated protein, Pgk1, showed no change in protein abundance.

Glucose transporter downregulation is an adaptive response. In principle, the downregulation of glucose transporters could reflect an adverse consequence of arsenic, a protective response, or an irrelevant epiphenomenon. To test these possibilities, we employed an *hxt1-7*Δ mutant (16), which is unable to grow with glucose as the sole carbon source but which grows well if provided another carbon source (e.g., maltose) which can be imported by other transporters. In lacking all seven glucose transporters, it effectively mimics—and, indeed, exaggerates to its extreme—the process of glucose transporter downregulation. The *hxt1-7*Δ mutant was strongly resistant to arsenic treatment (Fig. 1C), growing robustly even at arsenite concentrations as high as 5 mM. By comparison, a previous genome-wide screen to identify arsenic-resistant mutants was carried out at 1 mM (20). This result suggests that glucose transporter downregulation is an adaptive cellular response to arsenic toxicity.

Glucose transporter downregulation is mediated by vacuolar degradation. The observed transporter downregulation could reflect either a transcriptional or a post-

transcriptional response. To examine transcription, we performed reverse transcription-PCR (RT-PCR). *HXT2* showed a very slight decrease in mRNA abundance after arsenite treatment, while *HXT6* and *HXT7* actually showed slightly increased mRNA abundance (Fig. 2A). Thus, downregulation at the protein level is unlikely to be explained by a transcriptional effect. We next considered whether protein degradation could account for the arsenic-dependent loss of Hxt2 and Hxt7. In eukaryotes, there are two major pathways of protein degradation, which are mediated by the proteasome and the lysosome, respectively. The proteasome is a 2.5-MDa multisubunit complex that is found in the nucleus and the cytoplasm and that is associated with membranes (21, 22). The lysosome, in contrast, is a membrane-bound organelle that houses large quantities of proteases within its lumen (in yeast, the lysosome is also referred to as the vacuole). Degradation by both the proteasome and the vacuole is frequently signaled by the covalent attachment of the small protein ubiquitin to the target protein (23). To block proteasome-mediated degradation, we employed bortezomib (Velcade), a widely used small-molecule inhibitor of the proteasome. We pretreated cells with bortezomib and then treated them with arsenic to induce the downregulation of the Hxt proteins. The efficacy of proteasome inhibition was confirmed by the strong accumulation of high-molecular-weight ubiquitin-immunoreactive material as well as a specific proteasome substrate, Tmc1 (Fig. 2B; compare the first and third lanes) (24). In contrast, Hxt7 downregulation was completely unaffected by proteasome inhibition (Fig. 2B). Similar results were obtained for Hxt2 (Fig. 2C). These results suggest that arsenic-dependent downregulation of Hxt2 and Hxt7 is independent of the proteasome.

To determine whether vacuolar degradation might be responsible for glucose transporter downregulation, we employed the *doa4*Δ mutant. Doa4 acts at a late stage of vacuolar degradation (25). As a deubiquitinating enzyme, it removes ubiquitin from vacuolar substrates, an apparently obligate step for the trafficking and degradation of many such substrates. Both Hxt2 and Hxt7 were strongly stabilized in this mutant (Fig. 2D and E). These results suggest that vacuolar degradation is likely to account for arsenic-induced degradation of these glucose transporters. An important caveat to this interpretation is that, owing to its molecular defect, the *doa4*Δ mutant is also deficient in cellular levels of free ubiquitin (26), which could, in principle, indirectly stabilize some substrates. We therefore examined two other mutants deficient in vacuolar degradation which are not known to be ubiquitin deficient, *vps36*Δ and *vps25*Δ, both of which are part of the ESCRT-II complex (27). Hxt7 was strongly stabilized in both mutants after arsenic treatment (Fig. 2F). Both mutants also showed a significant growth defect upon arsenic treatment (Fig. 2G), consistent with an important physiologic role for these proteins in the cellular response to arsenic.

Ubiquitin-dependent degradation of glucose transporters. As mentioned above, vacuolar degradation, particularly of membrane proteins, is frequently signaled by the process of ubiquitination. The process of ubiquitination occurs by the sequential action of the E1, E2, and E3 enzymes. In yeast, there is a single E1 enzyme, 11 E2 enzymes, and >100 E3 enzymes, which allow for a hierarchical organization of these pathways (28). We sought to determine the E2 enzyme for this process. In previous work, we had determined the arsenite sensitivities of seven E2 null mutants (mutants lacking *rad6* and *ubc4*, *-5*, *-7*, *-8, -11*, and *-13*) (24). Only the *ubc4*Δ mutant showed a strong growth defect upon arsenic treatment, suggesting an important role for Ubc4 in the response to arsenic (24). Interestingly, Ubc5, which is highly similar to Ubc4 at the amino acid level (29), showed no such phenotype. We therefore began by testing Ubc4 and Ubc5. We observed a striking degradation defect for Hxt7 in the *ubc4*Δ mutant but not in the *ubc5*Δ mutant (Fig. 3A). Consistent with our prior data, the *ubc4*Δ mutant but not the *ubc5*Δ mutant showed strong sensitivity to arsenite (Fig. 3B). Interestingly, Hxt2 was not stabilized in either the *ubc4*Δ or the *ubc5*Δ mutant (data not shown). This could reflect either the known functional redundancy of Ubc4/5 or a different E2 requirement for Hxt2 degradation in response to arsenic.

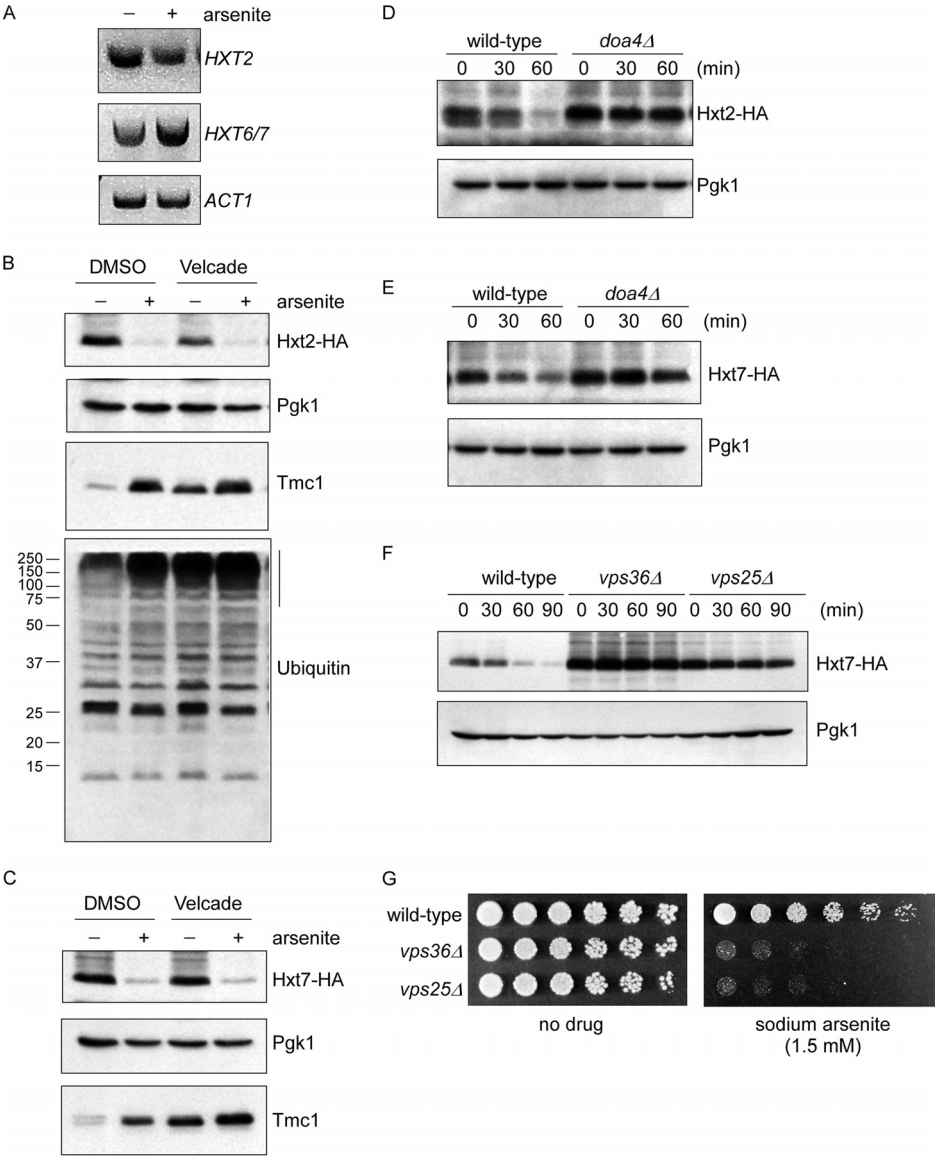

FIG 2 Vacuolar degradation mediates arsenic-induced glucose transporter downregulation. (A) The mRNA levels of the indicated hexose transporters before (lanes −) and 1 h after (lanes +) treatment with sodium arsenite (1 mM) were determined by RT-PCR. Actin (*ACT1*) served as a loading control. *HXT6* and *HXT7* differ at only 3 codons (1 amino acid) and so are amplified together by the same primer set. (B) Arsenic-induced downregulation of Hxt2-HA persists in the presence of proteasome inhibitors. Cells were pretreated with dimethyl sulfoxide (DMSO) or bortezomib (Velcade; 30 μM) to inhibit the proteasome and then treated with sodium arsenite (1 mM) for 1 h. Whole-cell extracts were prepared and analyzed by SDS-PAGE, followed by immunoblotting with the indicated antibodies. Pgk1 served as a loading control. Ubiquitin and the known proteasome substrate Tmc1 served to verify the efficiency of proteasome inhibition. This experiment was carried out in the *pdr5*Δ mutant background to increase the intracellular levels of bortezomib. Note that arsenic alone induces strong proteotoxic effects, as indicated by the increase in both high-molecular-weight ubiquitinated material and Tmc1 (compare the first and second lanes), consistent with prior reports (24, 49). Numbers on the left are molecular masses (in kilodaltons). (C) Arsenic-induced downregulation of Hxt7-HA persists in the presence of proteasome inhibitors. Cells were pretreated with DMSO or bortezomib (100 μM) to inhibit the proteasome and then treated with sodium arsenite (1 mM) for 2 h. Whole-cell extracts were prepared and analyzed by SDS-PAGE, followed by immunoblotting with the indicated antibodies. As in panel B, Pgk1 served as a loading control and Tmc1 served to verify the efficiency of proteasome inhibition. This experiment was carried out in the *pdr5*Δ mutant background to increase the intracellular levels of bortezomib. (D and E) Stabilization of Hxt2-HA (D) and Hxt7-HA (E) in the *doa4*Δ mutant. Wild-type and *doa4*Δ mutant cells were treated with sodium arsenite (1 mM), and whole-cell extracts were prepared at the indicated time points and analyzed by SDS-PAGE and immunoblotting. (Top) Anti-HA antibody; (bottom) Pgk1 (loading control). (F) Stabilization of Hxt7-HA in response to sodium arsenite in the *vps36*Δ and *vps25*Δ vacuolar degradation mutants. The experiment was conducted analogously to the experiments whose results are shown in panels D and E. (G) Growth of the wild-type, *vps36*Δ, and *vps25*Δ strains in the presence or absence of 1.5 mM sodium arsenite. Cells were spotted in a 3-fold dilution series and incubated at 30°C for 2 days.

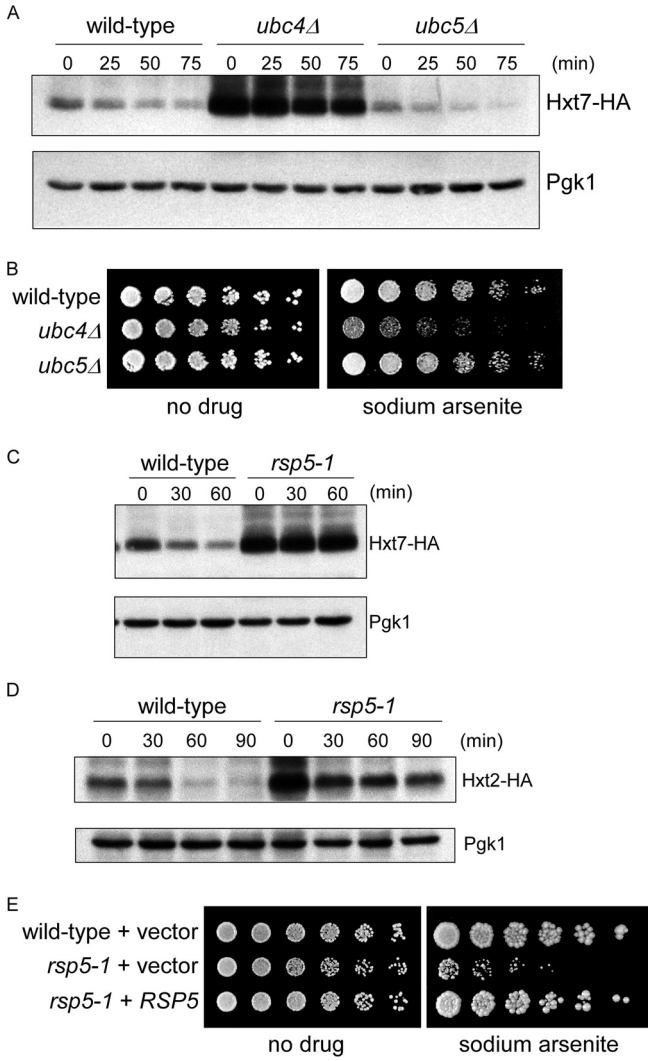

FIG 3 Arsenic-induced glucose transporter degradation requires Ubc4 and Rsp5. (A) Degradation of Hxt7-HA in the wild-type, *ubc4*Δ, and *ubc5*Δ strains in response to sodium arsenite (1 mM). Whole-cell extracts were prepared at the indicated time points and analyzed by SDS-PAGE and immunoblotting. (Top) Anti-HA antibody; (bottom) Pgk1 (loading control). (B) Growth of the wild-type, *ubc4*Δ, and *ubc5*Δ strains in the presence or absence of sodium arsenite (1.5 mM). Cells were spotted in a 3-fold serial dilution series and incubated at 30°C for 2 to 3 days. (C) Degradation of Hxt7-HA in the wild type and the temperature-sensitive *rsp5-1* mutant in response to sodium arsenite (1 mM). Whole-cell extracts were prepared at the indicated time points and analyzed by SDS-PAGE and immunoblotting. (Top) Anti-HA antibody; (bottom) Pgk1 (loading control). The experiment was performed at 30°C. (D) Degradation of Hxt2-HA in the wild type and the temperature-sensitive *rsp5-1* mutant in response to sodium arsenite (1 mM). Whole-cell extracts were prepared at the indicated time points and analyzed by SDS-PAGE and immunoblotting. (Top) Anti-HA antibody; (bottom) Pgk1 (loading control). Note that the restrictive temperature used here (37°C) was higher than that used in the experiment whose results are presented in panel C. (E) Growth of the wild type and the *rsp5-1* mutant expressing either an empty vector or the *RSP5* complementation plasmid, as indicated, in the presence or absence of sodium arsenite (1 mM). Cells were spotted in a 3-fold serial dilution series and incubated at 30°C for 2 (no drug) or 4 (arsenite) days.

Rsp5 is a highly active E3 enzyme responsible for most ubiquitination of plasma membrane proteins in yeast. It was therefore a prime E3 candidate, particularly since Rsp5 and Ubc4 are known to collaborate in the ubiquitination of some substrates (30, 31). Rsp5 is essential for viability, so we employed a well-studied temperature-sensitive mutant, the *rsp5-1* mutant (32). We observed a strong defect in the arsenic-induced downregulation of Hxt7 in this mutant (Fig. 3C). A strong stabilization of Hxt2 was also observed, but it was less complete and required a higher restrictive temperature (Fig. 3D). This suggests that Hxt2 may be a more permissive substrate of Rsp5, although the

possibility that other E3 enzymes contribute to its degradation is difficult to exclude. The *rsp5-1* mutant showed a striking survival defect upon arsenic treatment, again consistent with a critical role for Rsp5 in the cellular response to this drug (Fig. 3E). This defect could be complemented by the restoration of Rsp5 expression using a low-copy-number centromeric vector bearing the endogenous Rsp5 promoter (Fig. 3E).

K63-linked ubiquitin chains are required for arsenic-induced glucose transporter degradation. Ubiquitin may be transferred to target proteins as a monomer (monoubiquitination). However, because ubiquitin itself harbors seven lysine residues (K6, K11, K27, K29, K33, K48, K63), ubiquitination may also proceed through a polyubiquitin chain. Each chain adopts a structurally distinct conformation and, therefore, may signal different outcomes depending on how that ubiquitin chain is recognized within the cell (33). K48-linked chains, for example, frequently serve to promote degradation at the proteasome, while K63-linked chains have been implicated in a variety of stress response pathways that comprise both nondegradative and degradative functions (33, 34).

We sought to determine the ubiquitin chain linkage required for arsenic-induced glucose transporter downregulation. In yeast, ubiquitin is encoded by four separate genes (*UBI1* to *UBI4*). We therefore used a strain in which all four ubiquitin genes had been deleted and the sole source of ubiquitin is plasmid derived (34). Mutation of each of ubiquitin's lysines (K6R, K11R, etc.) produces a strain specifically deficient in generating that ubiquitin chain linkage. The only exception is K48, as the K48R mutation is not viable. Importantly, expression levels in this strain approximate physiologic ubiquitin levels.

We began by examining the phenotypic sensitivity of each ubiquitin K-to-R mutant upon arsenic exposure. Four of the chain linkages (K11, K27, K29, K33) appeared to be completely dispensable for survival on arsenic (Fig. 4A). In contrast, the K63R mutant showed a pronounced survival defect, while the K6R mutant showed a lesser defect. The latter effect was of particular interest, given that the K6 linkage remains poorly understood.

We next looked directly at arsenic-induced transporter degradation, focusing on the K6 and K63 mutants. Both Hxt2 and Hxt7 were strongly stabilized in the K63R mutant but not in the K6R mutant (Fig. 4B and C). This is consistent with prior work showing that Rsp5 can elaborate K63-linked chains in at least some contexts (35, 36), although in other contexts Rsp5 synthesizes K48-linked chains (37). The basis for the K6R mutant's sensitivity to arsenic remains unknown.

Identification of arsenic-dependent ubiquitination sites within Hxt2 and Hxt7. We sought to identify the arsenic-dependent ubiquitination sites within Hxt2 and Hxt7. Both proteins are 12-transmembrane-domain proteins. Hxt2 contains 17 lysines within its cytoplasmic domains, while Hxt7 contains 19 lysines (Fig. 5A and B). This obviously presents a formidable challenge for site-directed mutagenesis. To address this challenge, we took a second proteomics approach. Ubiquitin ends with the residues Arg-Gly-Gly. After trypsin digestion of an extract, proteins that had been previously modified by ubiquitin remain modified by the GG remnant of the ubiquitin that had been attached to the substrate's acceptor lysine residue. These so-called KGG peptides can be enriched by affinity purification with an anti-GG antibody and then quantitated by isobaric-labeling mass spectrometry (38, 39). We used this approach to determine the ubiquitinated proteome at 0, 1, and 4 h after arsenic treatment.

Our results indicate a comprehensive and dynamic program of ubiquitination in response to arsenic treatment. We quantitated 4,125 unique ubiquitinated peptides, representing 1,794 unique proteins (see Table S3 in the supplemental material). We also quantified the total protein abundance in parallel, which allowed us to normalize ubiquitinated peptide abundance to overall protein levels, providing a more specific readout of ubiquitination (Fig. 5C). Principal-component analysis revealed a very high degree of concordance between the three biological replicates as well as separation between treatment groups (Fig. 5D). This was reflected in the generally high repro-

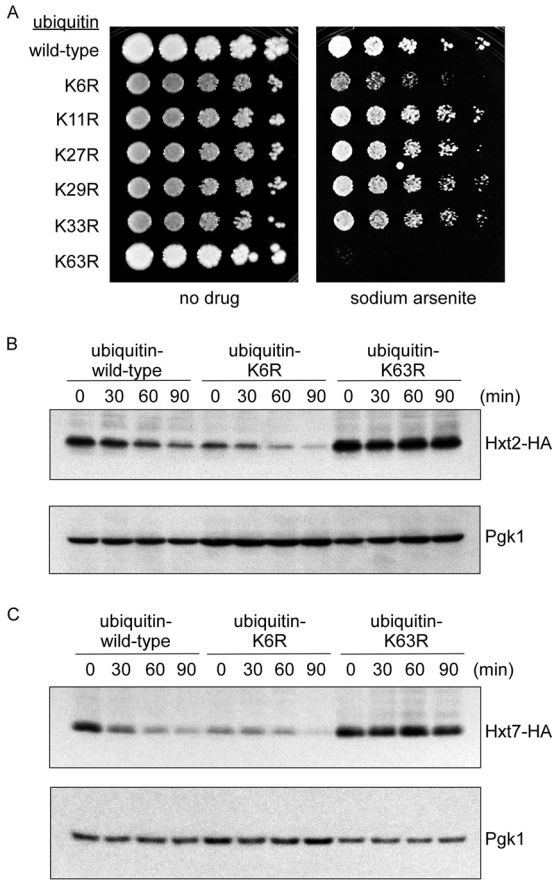

FIG 4 Arsenic-induced degradation of Hxt2 and Hxt7 requires K63 ubiquitin chain linkages. (A) Growth of the wild type and the six indicated ubiquitin mutants in the presence or absence of sodium arsenite (1.5 mM). Cells were spotted in a 3-fold serial dilution series and incubated at 30°C for 2 to 3 days. (B and C) Degradation of Hxt2-HA or Hxt7-HA in strains unable to generate K6 or K63 ubiquitin chain linkages in response to trivalent arsenic (1 mM). Whole-cell extracts were prepared at the indicated time points and analyzed by SDS-PAGE and immunoblotting. (Top) Anti-HA antibody; (bottom) Pgk1 (loading control).

ducibility for individual ubiquitinated peptides across replicates, as well as the very different ubiquitination profiles at 0, 1, and 4 h after treatment (Fig. 5C and D).

Several patterns of ubiquitination were evident in the proteomic data. Some peptides showed a progressive increase in ubiquitination over the time course, while others showed a progressive decrease in ubiquitination. Many others, in contrast, showed a burst of ubiquitination at 1 h followed by a return toward the baseline at 4 h (Fig. 5C). We also detected all 7 ubiquitin linkage types. Many of these, including K48 and K63, recapitulated this dynamic behavior, spiking at 1 h and then moving back toward the baseline at 4 h (Fig. 5E). We confirmed this result by standard immunoblotting. There was a strong increase in high-molecular-weight ubiquitinated material at 1 h after arsenic treatment, but at 4 h this response had largely normalized (Fig. 5F).

Ubiquitinated peptides corresponding to Hxt2 and Hxt7 were detected. For Hxt2, three ubiquitinated peptides centered on K37, K257, and K534/536 were identified (Fig. 5G). For Hxt7, a single cytoplasmic ubiquitinated peptide centered on K40 was identified (Fig. 5H). For both proteins, ubiquitination was dynamic, showing a burst at 1 h followed by a return to near baseline levels (Fig. 5G and H). This likely reflects that early ubiquitination events are efficient in promoting degradation, limiting the need for further ubiquitination later in the time course.

We started with Hxt2 and mutated K37, K257, K534, and K536 to arginine. This mutant showed a wild-type rate of arsenic-induced degradation (data not shown). We

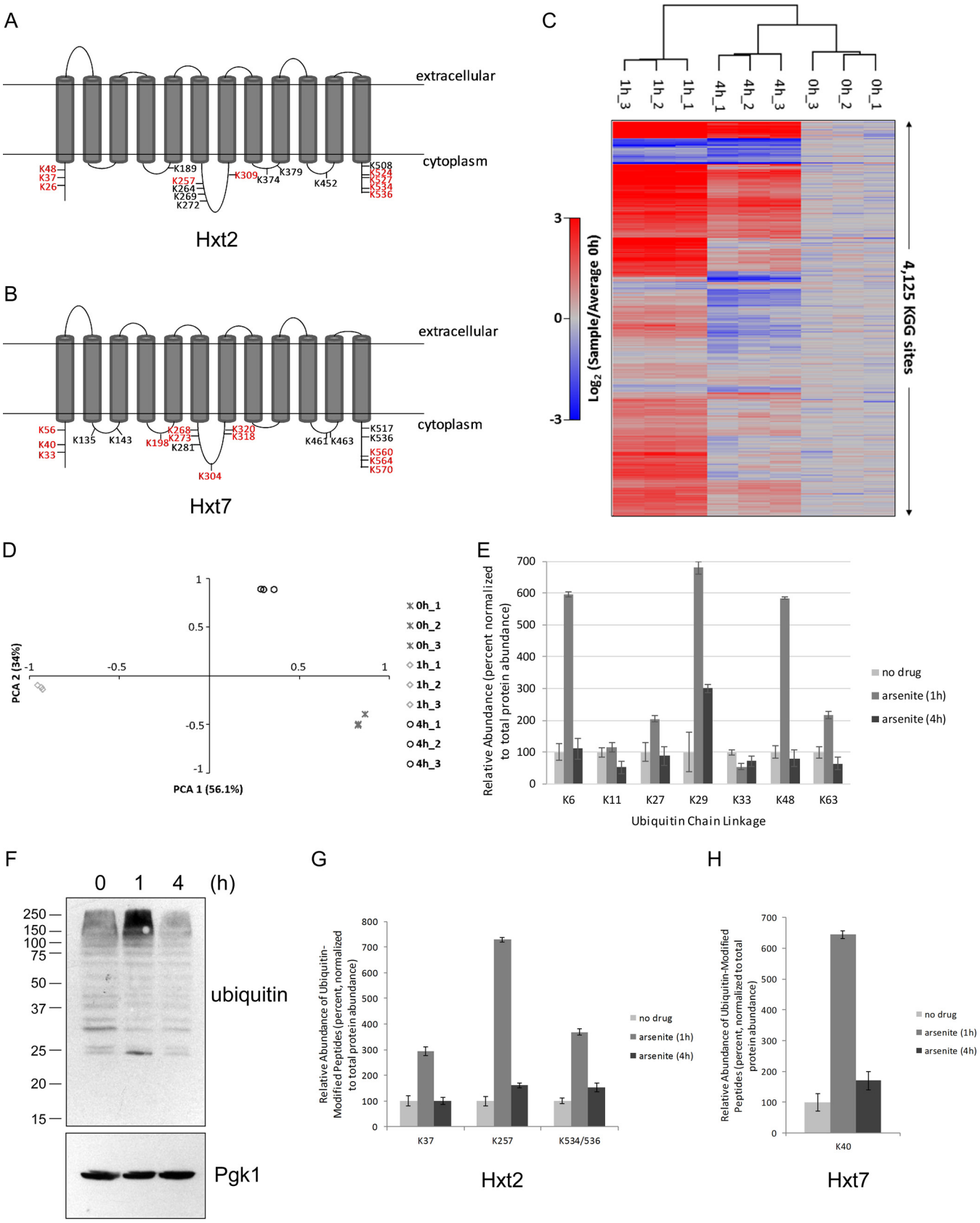

FIG 5 Determination of the ubiquitinated proteome after arsenite treatment. (A and B) Schematic illustration of Hxt2 (A) and Hxt7 (B). The approximate positions of the 17 (Hxt2) and 19 (Hxt7) cytoplasmic lysines, which are potential ubiquitination sites, are indicated. Residues mutated in the Hxt2-9K-to-R and Hxt7-12K-to-R mutants (see Fig. 6) are shown in red. (C) Heat map representation of the relative change in abundance of ubiquitinated peptides at 0, 1, and

(Continued on next page)

considered that nearby lysine residues might be capable of supporting ubiquitination. We further mutated K524 and K527 in the final cytoplasmic segment, but this mutant continued to display significant degradative rates (Fig. 6A, 6K-to-R mutant). However, upon mutating K26 and K48 (near K37) and K309 (near K257), we observed a strong stabilization of Hxt2 in response to arsenic treatment (Fig. 6A, 9K-to-R mutant). Similar behavior was observed with Hxt7. A K40R mutant showed wild-type rates of degradation (data not shown). However, further mutation of the N- and C-terminal cytoplasmic domains, as well as the larger central cytoplasmic loop (12K-to-R mutant), resulted in strong stabilization of the protein (Fig. 6B).

Given the number of mutations introduced, we sought to determine whether the stabilized Hxt2 and Hxt7 proteins retained their function as glucose transporters. To do this, we expressed wild-type Hxt2 and the stabilized Hxt2-9K-to-R mutant in the *hxt1-7*Δ mutant background. Since the *hxt1-7*Δ mutant cannot grow on glucose-containing media, any growth conferred by these plasmids indicates the restoration of glucose transport. The Hxt2-9K-to-R mutant grew as well as cells with wild-type Hxt2 (Fig. 6C). Similarly, the Hxt7-12K-to-R mutant grew as well as or even slightly better than cells with wild-type Hxt7 (Fig. 6D).

The preceding results suggest that degradation of glucose transporters may protect cells against arsenic toxicity. To test this hypothesis directly, we expressed the Hxt2 wild-type and Hxt2-9K-to-R plasmids in the *hxt1-7*Δ mutant, which is resistant to arsenic. Arsenic resistance was largely preserved upon restoration of wild-type Hxt2 (Fig. 6E). In contrast, introduction of the degradation-resistant 9K-to-R mutant restored arsenic sensitivity to the *hxt1-7*Δ mutant (Fig. 6E). Finally, we looked at the normalization of high-molecular-weight ubiquitin conjugates after arsenic treatment. The Hxt2-9K-to-R mutant showed a slower normalization of ubiquitin conjugates than the Hxt2-wild-type strain (Fig. 6F). These data are consistent with a protective role for glucose transporter degradation in the cellular response to arsenic.

DISCUSSION

A novel pathway of arsenic-induced degradation of glucose transporters. We have described a novel pathway by which cells destroy glucose transporters in response to arsenite exposure. This ubiquitin-dependent degradation occurs in the vacuole, requires the function of Ubc4 and Rsp5, and is mediated by K63-linked ubiquitin chains. The protective nature of this response is indicated in three ways. First, a mutant lacking all 7 glucose transporters is strongly resistant to arsenic. Second, all of the mutants deficient in glucose transporter degradation (including the *vps25*Δ, *vps36*Δ, *ubc4*Δ, *rsp5-1*, and ubiquitin-K63R mutants) are sensitive to arsenite. Third, and most importantly, a mutant of Hxt2 compromised for arsenic-induced degradation restores arsenic sensitivity to the *hxt1-7*Δ mutant. What is the molecular basis for this protective effect? Previous work suggests that glucose transporters are major mediators of arsenic import (15, 18, 19), providing a potential molecular rationale for this response. Another possibility, which is not mutually exclusive, concerns the recently described pathway of plasma membrane quality control. This pathway is also mediated by Rsp5 and targets misfolded membrane proteins to the vacuole for degradation (40). This pathway has been studied primarily under conditions of heat shock. Arsenic is a

FIG 5 Legend (Continued)
4 h after arsenic treatment (1 mM). The three columns per time point represent biological triplicates. A total of 4,125 peptides representing 1,794 unique proteins were quantitated. The results shown here have been normalized to total protein abundance, which was determined in parallel, to provide a more specific readout of arsenic-induced ubiquitination. (D) Principal-component analysis (PCA) of the proteomic data set shown in panel C. Individual points represent the three biological triplicates, confirming a high degree of concordance between triplicates as well as very different ubiquitinated proteomes at 0, 1, and 4 h after arsenic treatment. (E) Relative abundance of the seven ubiquitin chain linkage types after arsenite treatment, as determined by proteomic analysis. Data have been normalized to total ubiquitin abundance. Sodium arsenite treatment was at 1 mM for the indicated times. Error bars reflect standard deviations for biological triplicates. (F) Dynamic changes in the accumulation of high-molecular-weight ubiquitin-immunoreactive material after sodium arsenite treatment (1 mM). Whole-cell extracts were prepared at the indicated time points and analyzed by SDS-PAGE and immunoblotting. (Top) Antiubiquitin antibody; (bottom) Pgk1 (loading control). Numbers on the left are molecular masses (in kilodaltons). (G and H) Relative abundance of all detected cytoplasmic ubiquitinated peptides from Hxt2 and Hxt7, as determined by the proteomic analysis whose results are presented in panel C. Error bars represent standard deviations for triplicate cultures.

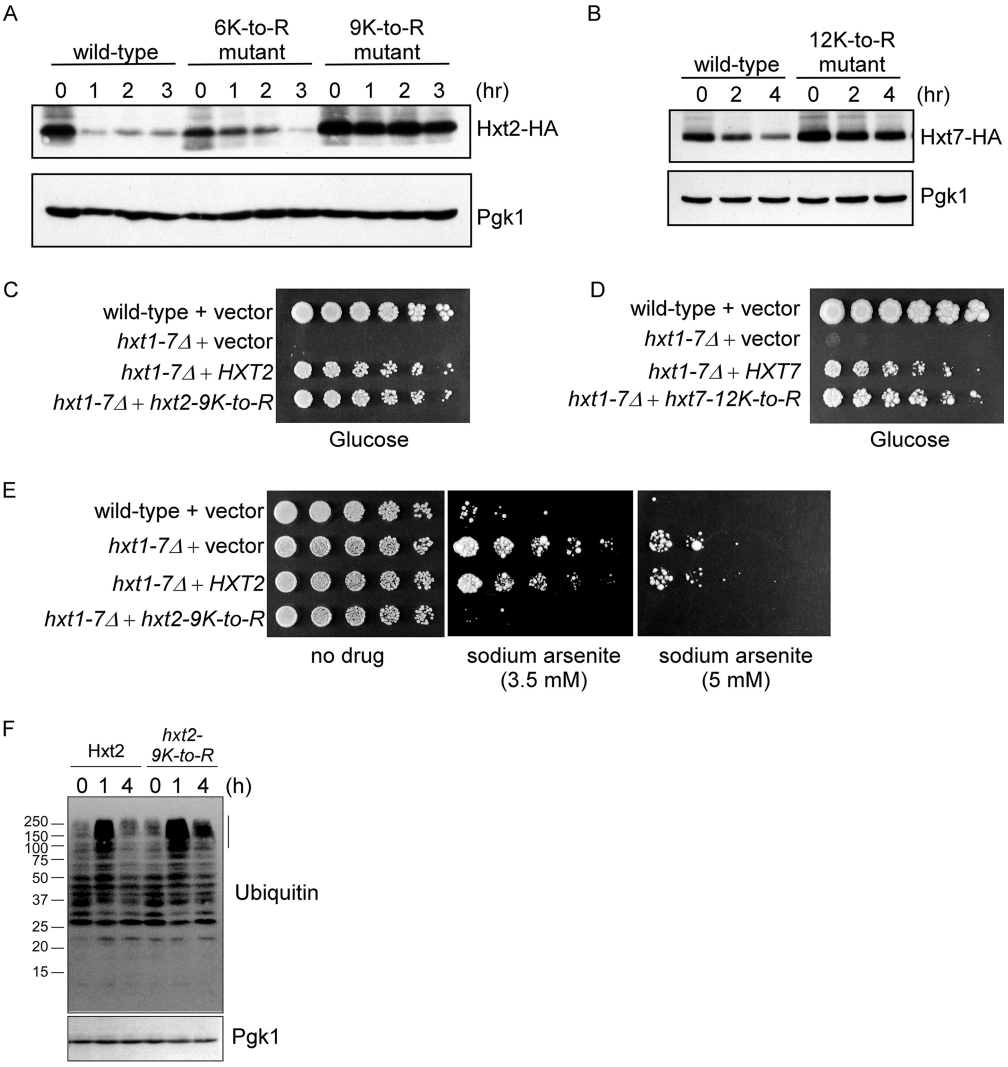

FIG 6 Identification of ubiquitination sites in Hxt2 and Hxt7 for arsenic-induced protein degradation. (A) Degradation of the wild type and lysine-to-arginine mutants of Hxt2 in response to sodium arsenite (1 mM). The 6K-to-R mutant affects lysines 37, 257, 524, 527, 534, and 536. The 9K-to-R mutant additionally affects lysines 26, 48, and 309. Whole-cell extracts were prepared at the indicated time points and analyzed by SDS-PAGE and immunoblotting. (Top) Anti-HA antibody; (bottom) Pgk1 (loading control). (B) Degradation of the wild type and the lysine-to-arginine mutants of Hxt7 in response to sodium arsenite (1 mM). The 12K-to-R mutant affects lysines 33, 40, 56, 198, 268, 273, 304, 318, 320, 560, 564, and 570. Whole-cell extracts were prepared at the indicated time points and analyzed by SDS-PAGE and immunoblotting. (Top) Anti-HA antibody; (bottom) Pgk1 (loading control). (C) Growth of the wild type and the *hxt1-7*Δ mutant expressing plasmids harboring an empty vector, wild-type Hxt2, and the Hxt2-9K-to-R mutant on medium containing glucose as the sole carbon source. Cells were spotted in a 3-fold serial dilution series and incubated at 30°C for 6 days. (D) Growth of the wild type and the *hxt1-7*Δ mutant expressing plasmids harboring an empty vector, wild-type Hxt7, and the Hxt7-12K-to-R mutant on medium containing glucose as the sole carbon source. Cells were spotted in a 3-fold serial dilution series and incubated at 30°C for 6 days. (E) Growth of the wild type and the *hxt1-7*Δ mutant expressing plasmids harboring an empty vector, wild-type Hxt2, and the Hxt2-9K-to-R mutant on medium containing or lacking sodium arsenite, as indicated. Cells were spotted in a 3-fold serial dilution series and incubated at 30°C for 3 days (no drug), 9 days (3.5 mM arsenite), or 14 days (5 mM arsenite). Note that this experiment was performed in rich medium with maltose as the sole carbon source to minimize any beneficial effects related to glucose uptake by Hxt2 proteins. (F) Dynamic changes in the accumulation of high-molecular-weight ubiquitin-immunoreactive material in *hxt1-7*Δ cells expressing either wild-type Hxt2 or the Hxt2-9K-to-R mutant. Sodium arsenite treatment was at 1 mM for the indicated times. Whole-cell extracts were prepared at the indicated time points and analyzed by SDS-PAGE and immunoblotting. (Top) Antiubiquitin antibody; (bottom) Pgk1 (loading control). The effect of the Hxt2-9K-to-R mutant was the most pronounced in the high-molecular-weight range, indicated by a line to the right of the panel. Numbers on the left are molecular masses (in kilodaltons).

potent inducer of proteotoxic stress (9) and therefore might be capable of activating this pathway.

The other major mediator of arsenic import in yeast is the glycerol channel Fps1 (14). Fps1 function is also inhibited in response to arsenic. In contrast to the glucose

transporters, our proteomic analysis did not reveal strong degradation of Fps1 (9). This is consistent with previous work highlighting a distinct mechanism of Fps1 regulation in response to arsenic. Arsenic exposure leads to phosphorylation of Rgc2, a positive regulator of Fps1 (41–43). This causes dissociation of Rgc2 from Fps1, resulting in the loss of Fps1 transport function. Thus, cells have developed diverse and complex mechanisms to limit arsenic import. Indeed, these responses are only part of a larger detoxification program involving arsenic efflux, chemical modification, and sequestration (1, 5). The complexity of this program underscores the evolutionary importance of the threat posed by environmental arsenic exposure.

The defect in arsenic-induced degradation of Hxt2 and Hxt7 in many of the mutants described here (including the *ubc4*Δ, *rsp5-1*, and vacuolar mutants) is accompanied by an increase in the steady-state abundance of the glucose transporters. This increase in steady-state Hxt2 and Hxt7 levels may contribute to the arsenic sensitivity of each of these mutants. Moreover, this observation implies that these transporters are subject to some degree of basal turnover even under normal conditions and that there is significant overlap in the molecular machinery involved in the arsenic-induced and basal pathways of degradation. Still other pathways of glucose transporter degradation have been previously described, the best characterized being in response to glucose availability. Glucose-induced degradation also occurs in the vacuole and requires Ubc4 and Rsp5 (16, 44–47). Thus, although glucose transporter degradation may be signaled by different inputs, there appear to be key components of the respective degradative pathways that are shared.

Mechanistic basis for arsenic-induced glucose transporter degradation. Arsenite is a potent inducer of glucose transporter degradation. However, the mechanism by which arsenic signals degradation remains unknown. An important aspect of arsenic function is its ability to covalently bind to free thiol groups within amino acid side chains (10–11). An intriguing possibility, then, is that arsenic directly binds to glucose transporters, resulting in a chemical or structural change that triggers degradation. In general, the higher-affinity transporters showed an increased degree of arsenic-induced degradation (Fig. 1A). If arsenic did bind these proteins directly, its relative affinity for different transporters might then explain this differential effect. A second possibility is that a more conventional second messenger signaling pathway mediates degradation. Arsenic-induced phosphorylation of glucose transporters, for example, could trigger ubiquitination and subsequent degradation. If so, the question of how arsenic induces phosphorylation would still require explanation. Finally, it is possible that arsenic somehow co-opts the well-established glucose-dependent pathway of transporter degradation. This could explain the affinity-dependent differences in transporter degradation. Multiple glucose sensors exist, including Rgt2 and Snf3, although their known functions primarily relate to transcriptional regulation (17), which does not seem to be critical for the arsenic-induced pathway of downregulation. Further work will be needed to distinguish between these and still other possible mechanisms.

The ubiquitinated proteome in response to arsenite. Our previous proteomic analysis of the cellular response to arsenite suggested a comprehensive remodeling of the proteome, with approximately 1,000 proteins showing a significant change in protein abundance (9). Pathways related to protein synthesis, folding, and degradation were particularly affected, indicating the relevance of arsenic to protein homeostasis. Here we have specifically determined the ubiquitinated proteome under similar conditions. The results are remarkable in at least two ways. The first is the sheer scope of ubiquitin-dependent cellular regulation induced by arsenic. Nearly 1,800 proteins were ubiquitinated in response to arsenic, representing approximately 30% of all proteins in yeast. Second, the TMT method's increased capacity for multiplexing allowed us to measure ubiquitination at multiple time points, revealing dynamic aspects of ubiquitination that would not have been apparent with a more traditional treated-versus-untreated approach. For many substrates, there was a clear burst of ubiquitination at 1 h, followed by normalization at 4 h. The precise relationship between these ubiquitin

conjugates and arsenic toxicity is not entirely clear, but the dynamic behavior observed does suggest that, for at least some processes, early ubiquitination events are effective in achieving certain cellular outcomes. The fact that we simultaneously quantitated total protein abundance within the same experiment allows for a correlation between protein ubiquitination and abundance for individual proteins. Although we focused our efforts on just two of the ubiquitinated proteins, Hxt2 and Hxt7, we expect that this database (see Table S3 in the supplemental material) will serve as a valuable resource to the community for future investigation.

Other aspects of the arsenic stress response also show this property of rapid normalization over time. We previously showed that the proteotoxic stress response mediated by Rpn4, which is best known for controlling proteasome abundance, is potently induced by arsenic at 1 h after treatment but then returns toward the baseline over several hours (9).

Finally, although K6-linked ubiquitination was not required for degradation of Hxt2 or Hxt7, the growth defect of the ubiquitin K6R mutant upon arsenite exposure is intriguing, given that this linkage type remains poorly understood. Further work to understand how the K6 linkage contributes in the cellular response to arsenic could shed light on this important aspect of ubiquitin signaling.

Implications for human disease. In addition to its well-established role as a carcinogen, a large body of epidemiologic evidence indicates a strong association between arsenic exposure and the risk for diabetes (3, 4), a conclusion supported by a comprehensive meta-analysis of the literature by the National Toxicology Program (2). However, the underlying molecular basis for this association remains unknown. The stimulation of glucose import into cells represents a critical aspect of insulin signaling. Failure to properly regulate glucose import results in hyperglycemia, which is a key feature of diabetes and related disorders, including prediabetic insulin resistance and the metabolic syndrome. It is unknown whether arsenic similarly induces the degradation of human glucose transporters, but there is evidence that mammalian Glut1 is capable of importing arsenic, similar to its yeast counterparts (18, 19). If mammalian glucose transporters are subject to arsenic-induced downregulation/degradation, this could represent a potentially compelling explanation for the epidemiologic link between arsenic and diabetes: arsenic exposure, by promoting glucose transporter degradation, could antagonize insulin's ability to promote glucose import, contributing to hyperglycemia, insulin resistance, and diabetes.

MATERIALS AND METHODS

Strains and plasmids. The yeast strains and plasmids used in this study are listed in Tables S1 and S2 in the supplemental material, respectively. Standard techniques were used for strain construction and plasmid transformation. Cells were cultured at 30°C, except for the experiment whose results are described in Fig. 3D, which was performed at 37°C. YPD medium consisted of 1% yeast extract, 2% Bacto peptone, and 2% dextrose. YPDM medium additionally contained 2% maltose. YPM medium was similar to YPD, but it contained 2% maltose instead of dextrose. Synthetic medium consisted of 0.7% Difco yeast nitrogen base, 2% dextrose and was supplemented with adenine, uridine, and amino acids. Plasmid selection was either by omission of uridine from the synthetic medium or by supplementation of the rich medium with nourseothricin (ClonNAT; 100 μg/ml), as appropriate.

pJH62 is a nourseothricin-selectable centromeric vector that was constructed by replacing the TRP1 marker in ycPlac22 (48) with the NAT-MX6 cassette.

Single site-directed mutagenesis was performed using the QuikChange method (Agilent). Multiple mutations were introduced simultaneously using the QuikChange multisite method (Agilent). The mutations were verified by sequencing.

Proteomic analysis. Relative changes in protein abundance upon arsenite exposure (1 mM) were previously determined using tandem mass tag (TMT)-based mass spectrometry (9). This experiment was done with biological triplicates and at three time points (0, 1, and 4 h). A total of 4,563 proteins were quantitated. The methods have been previously described in detail (9). The data shown in Fig. 1A represent those obtained from a further original analysis of that data set.

Quantitation of the ubiquitinated proteome was performed under similar conditions (i.e., biological triplicates sampled at 0, 1, and 4 h after arsenite treatment [1 mM]). The methods were largely similar to those used for the original proteomic analysis, except that di-Gly-containing peptides were first immunoprecipitated prior to TMT labeling (38). A total of 4,125 ubiquitinated peptides, representing a total of 1,794 proteins, were quantitated. Total protein abundance was determined in parallel, allowing for direct comparison between ubiquitinated peptides and total protein abundance. Briefly, yeast cells were lysed

by bead beating in 8 M urea, 50 mM HEPES, pH 7.3, 50 mM NaCl, and protease inhibitors. A total of 4 mg of protein was reduced and alkylated prior to digestion with Lys-C (3 h at 37°C) and trypsin (overnight at 37°C). Peptides were desalted with tC_{18} SepPak solid-phase extraction cartridges (Waters) and lyophilized. A di-Gly monoclonal antibody (32 μg/immunoprecipitation mixture [IP]; Cell Signaling Technology) was coupled to protein A Plus Ultralink resin (40 μl slurry/IP; Thermo Fisher Scientific) overnight at 4°C prior to its chemical cross-linking reaction. Peptides were resuspended in 1.5 ml of ice-cold IAP buffer (50 mM MOPS [morpholinepropanesulfonic acid; pH 7.2], 10 mM sodium phosphate, 50 mM NaCl), followed by centrifugation to remove any insoluble material. Supernatants (pH, ~7.2) were incubated with the antibody beads for 2 h at 4°C with gentle end-over-end rotation. Each lysate was immunoprecipitated twice. The flowthrough of each enrichment (100 μg) was saved for subsequent TMT labeling and data analysis (9). After centrifugation, beads were washed vigorously with IAP and phosphate-buffered saline buffers and eluted twice with 0.15% trifluoroacetic acid. Enriched di-Gly peptides were desalted, lyophilized, and labeled with TMT regents as described previously (38). All spectra were acquired on an Orbitrap Lumos mass spectrometer (Thermo Fisher Scientific) coupled to an Easy-nLC 1000 (Thermo Fisher Scientific) ultra-high-pressure liquid chromatography (UHPLC) pump. The Orbitrap Lumos parameters and data processing for both enriched di-Gly peptides and unbound peptides (protein levels) have been previously described in detail (9, 38).

RT-PCR. Reverse transcription-PCR (RT-PCR) was performed as previously described (24). *HXT2* was amplified using the primers 5′-GTCTGAATTCGCTACTAGCC-3′ and 5′-CCAGACGTCCTAAGGTTAAC-3′. *HXT6* and *HXT7* differ at only 3 codons (and at only 1 amino acid) and so were amplified together by use of the following primers: 5′-GTGTATCATGATCGCCTTTGG-3′ and 5′-GAAGGACCTTTGTCTTGCTAC-3′. *ACT1* was amplified with the primers 5′-CTGGTATGTTCTAGCGCTTG-3′ and 5′-GATACCTTGGTGTCTTGGTC-3′.

Protein degradation assays and immunoblot analysis. Whole-cell lysates were prepared from logarithmic-phase cultures that had been untreated or chemically treated as indicated above. Cells were normalized by optical density and collected by centrifugation. Pellets were resuspended in cold 2 M lithium acetate and incubated on ice for 5 min, followed by a 5-min incubation in cold 0.4 M sodium hydroxide on ice. After centrifugation, pellets were resuspended in 1× Laemmli buffer and boiled at 100°C for 5 min. Standard SDS-PAGE and immunoblotting were performed. Where indicated, cells were pretreated with bortezomib at the indicated concentrations for 1 h. These experiments were performed in the *pdr5*Δ mutant background to ensure high intracellular bortezomib concentrations.

The following antibodies were used in this study: anti-HA–peroxidase (catalog number 12013819001; Roche), anti-Pgk1 (catalog number 459250; Novex), anti-Tmc1 (24), and antiubiquitin (catalog number SC8017; Santa Cruz).

Phenotypic analysis. Overnight yeast cultures were normalized by optical density, spotted in a 3-fold serial dilution series on the plates indicated above, and cultured at 30°C.

SUPPLEMENTAL MATERIAL

Supplemental material for this article may be found at https://doi.org/10.1128/MCB.00559-18.

SUPPLEMENTAL FILE 1, PDF file, 0.2 MB.

SUPPLEMENTAL FILE 2, XLSX file, 1.9 MB.

ACKNOWLEDGMENTS

This work was supported by NIH grant DP5-OD019800 (to J.H.) and R01-GM067945 (to S.P.G.).

We thank Eckhard Boles and Chris Kaiser for yeast strains.

We report no financial conflicts of interest.

REFERENCES

1. Rosen BP, Liu Z. 2009. Transport pathways for arsenic and selenium: a minireview. Environ Int 35:512–515. https://doi.org/10.1016/j.envint.2008.07.023.
2. Maull EA, Ahsan H, Edwards J, Longnecker MP, Navas-Acien A, Pi J, Silbergeld EK, Styblo M, Tseng CH, Thayer KA, Loomis D. 2012. Evaluation of the association between arsenic and diabetes: a National Toxicology Program workshop review. Environ Health Perspect 120:1658–1670. https://doi.org/10.1289/ehp.1104579.
3. Bonini MG, Sargis RM. 2018. Environmental toxicant exposures and type 2 diabetes mellitus: two interrelated public health problems on the rise. Curr Opin Toxicol 7:52–59. https://doi.org/10.1016/j.cotox.2017.09.003.
4. Spratlen MJ, Grau-Perez M, Best LG, Yracheta J, Lazo M, Vaidya D, Balakrishnan P, Gamble MV, Francesconi KA, Goessler W, Cole SA, Umans JG, Howard BV, Navas-Acien A. 2018. The association of arsenic exposure and arsenic metabolism with the metabolic syndrome and its individual components: prospective evidence from the Strong Heart Family Study. Am J Epidemiol 187:1598–1612. https://doi.org/10.1093/aje/kwy048.
5. Yang HC, Fu HL, Lin YF, Rosen BP. 2012. Pathways of arsenic uptake and efflux. Curr Top Membr 69:325–358. https://doi.org/10.1016/B978-0-12-394390-3.00012-4.
6. Agency for Toxic Substances and Disease Registry, Centers for Disease Control and Prevention. 2017. ATSDR's substance priority list. https://www.atsdr.cdc.gov/spl/.
7. Hughes MF. 2002. Arsenic toxicity and potential mechanisms of action. Toxicol Lett 133:1–16. https://doi.org/10.1016/S0378-4274(02)00084-X.
8. Jacobson T, Navarrete C, Sharma SK, Sideri TC, Ibstedt S, Priya S, Grant CM, Christen P, Goloubinoff P, Tamás MJ. 2012. Arsenite interferes with protein folding and triggers formation of protein aggregates in yeast. J Cell Sci 125:5073–5083. https://doi.org/10.1242/jcs.107029.
9. Guerra-Moreno A, Isasa M, Bhanu MK, Waterman DP, Eapen VV, Gygi SP, Hanna J. 2015. Proteomic analysis identifies ribosome reduction as an effective proteotoxic stress response. J Biol Chem 290:29695–29706. https://doi.org/10.1074/jbc.M115.684969.
10. Rosen BP, Bhattacharjee H, Shi W. 1995. Mechanisms of metalloregulation of an anion-translocating ATPase. J Bioenerg Biomembr 27:85–91. https://doi.org/10.1007/BF02110335.

11. Shen S, Li XF, Cullen WR, Weinfeld M, Le XC. 2013. Arsenic binding to proteins. Chem Rev 113:7769–7792. https://doi.org/10.1021/cr300015c.
12. Rice KL, de Thé H. 2014. The acute promyelocytic leukaemia success story: curing leukaemia through targeted therapies. J Intern Med 276:61–70. https://doi.org/10.1111/joim.12208.
13. Zhang XW, Yan XJ, Zhou ZR, Yang FF, Wu ZY, Sun HB, Liang WX, Song AX, Lallemand-Breitenbach V, Jeanne M, Zhang QY, Yang HY, Huang QH, Zhou GB, Tong JH, Zhang Y, Wu JH, Hu HY, de The H, Chen SJ, Chen Z. 2010. Arsenic trioxide controls the fate of the PML-RARalpha oncoprotein by directly binding PML. Science 328:240–243. https://doi.org/10.1126/science.1183424.
14. Wysocki R, Chéry CC, Wawrzycka D, Van Hulle M, Cornelis R, Thevelein JM, Tamás MJ. 2001. The glycerol channel Fps1p mediates the uptake of arsenite and antimonite in Saccharomyces cerevisiae. Mol Microbiol 40:1391–1401. https://doi.org/10.1046/j.1365-2958.2001.02485.x.
15. Liu Z, Boles E, Rosen BP. 2004. Arsenic trioxide uptake by hexose permeases in Saccharomyces cerevisiae. J Biol Chem 279:17312–17318. https://doi.org/10.1074/jbc.M314006200.
16. Kruckeberg AL, Ye L, Berden JA, van Dam K. 1999. Functional expression, quantification and cellular localization of the Hxt2 hexose transporter of Saccharomyces cerevisiae tagged with the green fluorescent protein. Biochem J 339:299–307. https://doi.org/10.1042/0264-6021:3390299.
17. Ozcan S, Johnston M. 1999. Function and regulation of yeast hexose transporters. Microbiol Mol Biol Rev 63:554–569.
18. Liu Z, Sanchez MA, Jiang X, Boles E, Landfear SM, Rosen BP. 2006. Mammalian glucose permease GLUT1 facilitates transport of arsenic trioxide and methylarsonous acid. Biochem Biophys Res Commun 351:424–430. https://doi.org/10.1016/j.bbrc.2006.10.054.
19. Jiang X, McDermott JR, Ajees AA, Rosen BP, Liu Z. 2010. Trivalent arsenicals and glucose use different translocation pathways in mammalian GLUT1. Metallomics 2:211–219. https://doi.org/10.1039/B920471G.
20. Pan X, Reissman S, Douglas NR, Huang Z, Yuan DS, Wang X, McCaffery JM, Frydman J, Boeke JD. 2010. Trivalent arsenic inhibits the functions of chaperonin complex. Genetics 186:725–734. https://doi.org/10.1534/genetics.110.117655.
21. Finley D. 2009. Recognition and processing of ubiquitin-protein conjugates by the proteasome. Annu Rev Biochem 78:477–513. https://doi.org/10.1146/annurev.biochem.78.081507.101607.
22. Tomko RJ, Jr, Hochstrasser M. 2013. Molecular architecture and assembly of the eukaryotic proteasome. Annu Rev Biochem 82:415–445. https://doi.org/10.1146/annurev-biochem-060410-150257.
23. Piper RC, Luzio JP. 2007. Ubiquitin-dependent sorting of integral membrane proteins for degradation in lysosomes. Curr Opin Cell Biol 19:459–465. https://doi.org/10.1016/j.ceb.2007.07.002.
24. Guerra-Moreno A, Hanna J. 2016. Tmc1 is a dynamically regulated effector of the Rpn4 proteotoxic stress response. J Biol Chem 291:14788–14795. https://doi.org/10.1074/jbc.M116.726398.
25. Nikko E, André B. 2007. Evidence for a direct role of the Doa4 deubiquitinating enzyme in protein sorting into the MVB pathway. Traffic 8:566–581. https://doi.org/10.1111/j.1600-0854.2007.00553.x.
26. Swaminathan S, Amerik AY, Hochstrasser M. 1999. The Doa4 deubiquitinating enzyme is required for ubiquitin homeostasis in yeast. Mol Biol Cell 10:2583–2594. https://doi.org/10.1091/mbc.10.8.2583.
27. Teis D, Saksena S, Emr SD. 2009. SnapShot: the ESCRT machinery. Cell 137:182–182.e1. https://doi.org/10.1016/j.cell.2009.03.027.
28. Finley D, Ulrich HD, Sommer T, Kaiser P. 2012. The ubiquitin-proteasome system of Saccharomyces cerevisiae. Genetics 192:319–360. https://doi.org/10.1534/genetics.112.140467.
29. Seufert W, Jentsch S. 1990. Ubiquitin-conjugating enzymes UBC4 and UBC5 mediate selective degradation of short-lived and abnormal proteins. EMBO J 9:543–550. https://doi.org/10.1002/j.1460-2075.1990.tb08141.x.
30. Gwizdek C, Hobeika M, Kus B, Ossareh-Nazari B, Dargemont C, Rodriguez MS. 2005. The mRNA nuclear export factor Hpr1 is regulated by Rsp5-mediated ubiquitylation. J Biol Chem 280:13401–13405. https://doi.org/10.1074/jbc.C500040200.
31. Isasa M, Katz EJ, Kim W, Yugo V, González S, Kirkpatrick DS, Thomson TM, Finley D, Gygi SP, Crosas B. 2010. Monoubiquitination of RPN10 regulates substrate recruitment to the proteasome. Mol Cell 38:733–745. https://doi.org/10.1016/j.molcel.2010.05.001.
32. Helliwell SB, Losko S, Kaiser CA. 2001. Components of a ubiquitin ligase complex specify polyubiquitination and intracellular trafficking of the general amino acid permease. J Cell Biol 153:649–662. https://doi.org/10.1083/jcb.153.4.649.
33. Yau R, Rape M. 2016. The increasing complexity of the ubiquitin code. Nat Cell Biol 18:579–586. https://doi.org/10.1038/ncb3358.
34. Spence J, Sadis S, Haas AL, Finley D. 1995. A ubiquitin mutant with specific defects in DNA repair and multiubiquitination. Mol Cell Biol 15:1265–1273. https://doi.org/10.1128/MCB.15.3.1265.
35. Kee Y, Lyon N, Huibregtse JM. 2005. The Rsp5 ubiquitin ligase is coupled to and antagonized by the Ubp2 deubiquitinating enzyme. EMBO J 24:2414–2424. https://doi.org/10.1038/sj.emboj.7600710.
36. Erpapazoglou Z, Dhaoui M, Pantazopoulou M, Giordano F, Mari M, Léon S, Raposo G, Reggiori F, Haguenauer-Tsapis R. 2012. A dual role for K63-linked ubiquitin chains in multivesicular body biogenesis and cargo sorting. Mol Biol Cell 23:2170–2183. https://doi.org/10.1091/mbc.e11-10-0891.
37. Fang NN, Chan GT, Zhu M, Comyn SA, Persaud A, Deshaies RJ, Rotin D, Gsponer J, Mayor T. 2014. Rsp5/Nedd4 is the main ubiquitin ligase that targets cytosolic misfolded proteins following heat stress. Nat Cell Biol 16:1227–1237. https://doi.org/10.1038/ncb3054.
38. Rose CM, Isasa M, Ordureau A, Prado MA, Beausoleil SA, Jedrychowski MP, Finley DJ, Harper JW, Gygi SP. 2016. Highly multiplexed quantitative mass spectrometry analysis of ubiquitylomes. Cell Syst 3:395–403. https://doi.org/10.1016/j.cels.2016.08.009.
39. Fulzele A, Bennett EJ. 2018. Ubiquitin diGLY proteomics as an approach to identify and quantify the ubiquitin-modified proteome. Methods Mol Biol 1844:363–384. https://doi.org/10.1007/978-1-4939-8706-1_23.
40. Zhao Y, MacGurn JA, Liu M, Emr S. 2013. The ART-Rsp5 ubiquitin ligase network comprises a plasma membrane quality control system that protects yeast cells from proteotoxic stress. Elife 2:e00459. https://doi.org/10.7554/eLife.00459.
41. Thorsen M, Di Y, Tängemo C, Morillas M, Ahmadpour D, Van der Does C, Wagner A, Johansson E, Boman J, Posas F, Wysocki R, Tamás MJ. 2006. The MAPK Hog1p modulates Fps1p-dependent arsenite uptake and tolerance in yeast. Mol Biol Cell 17:4400–4410. https://doi.org/10.1091/mbc.e06-04-0315.
42. Lee J, Reiter W, Dohnal I, Gregori C, Beese-Sims S, Kuchler K, Ammerer G, Levin DE. 2013. MAPK Hog1 closes the S. cerevisiae glycerol channel Fps1 by phosphorylating and displacing its positive regulators. Genes Dev 27:2590–2601. https://doi.org/10.1101/gad.229310.113.
43. Lee J, Levin DE. 2018. Intracellular mechanism by which arsenite activates the yeast stress MAPK Hog1. Mol Biol Cell 29:1904–1915. https://doi.org/10.1091/mbc.E18-03-0185.
44. Krampe S, Boles E. 2002. Starvation-induced degradation of yeast hexose transporter Hxt7p is dependent on endocytosis, autophagy and the terminal sequences of the permease. FEBS Lett 513:193–196. https://doi.org/10.1016/S0014-5793(02)02297-4.
45. Krampe S, Stamm O, Hollenberg CP, Boles E. 1998. Catabolite inactivation of the high-affinity hexose transporters Hxt6 and Hxt7 of Saccharomyces cerevisiae occurs in the vacuole after internalization by endocytosis. FEBS Lett 441:343–347. https://doi.org/10.1016/S0014-5793(98)01583-X.
46. Snowdon C, van der Merwe G. 2012. Regulation of Hxt3 and Hxt7 turnover converges on the Vid30 complex and requires inactivation of the Ras/cAMP/PKA pathway in Saccharomyces cerevisiae. PLoS One 7:e50458. https://doi.org/10.1371/journal.pone.0050458.
47. Hovsepian J, Defenouillère Q, Albanèse V, Váchová L, Garcia C, Palková Z, Léon S. 2017. Multilevel regulation of an α-arrestin by glucose depletion controls hexose transporter endocytosis. J Cell Biol 216:1811–1831. https://doi.org/10.1083/jcb.201610094.
48. Gietz RD, Sugino A. 1988. New yeast-Escherichia coli shuttle vectors constructed with in vitro mutagenized yeast genes lacking six-base pair restriction sites. Gene 74:527–534. https://doi.org/10.1016/0378-1119(88)90185-0.
49. Guerra-Moreno A, Hanna J. 2017. Induction of proteotoxic stress by the mycotoxin patulin. Toxicol Lett 276:85–91. https://doi.org/10.1016/j.toxlet.2017.05.015.